

Article

Synthesis, Characterization, and Thin-Film Transistor Response of Benzo[i]pentahelicene-3,6-dione

Maria Paola Bracciale ^{1,*}, Guhyun Kwon ², Dongil Ho ², Choongik Kim ², Maria Laura Santarelli ¹
and Assunta Marrocchi ^{3,*}

¹ Department of Chemical Engineering Materials and Environment, University of Rome "Sapienza", Via Eudossiana 18, 00184 Rome, Italy; marialaura.santarelli@uniroma1.it

² Department of Chemical and Biomolecular Engineering, Sogang University, Seoul 04107, Korea; kguhyun1119@nate.com (G.K.); hdnel@naver.com (D.H.); choongik@sogang.ac.kr (C.K.)

³ Department of Chemistry, Biology and Biotechnology, University of Perugia, Via Elce di Sotto 8, 06123 Perugia, Italy

* Correspondence: mariapaola.bracciale@uniroma1.it (M.P.B.); assunta.marrocchi@unipg.it (A.M.); Tel.: +39-0644585563 (M.P.B.); +39-0755855536 (A.M.)

Abstract: Organic semiconductors hold the promise of simple, large area solution deposition, low thermal budgets as well as compatibility with flexible substrates, thus emerging as viable alternatives for cost-effective (opto)-electronic devices. In this study, we report the optimized synthesis and characterization of a helically shaped polycyclic aromatic compound, namely benzo[i]pentahelicene-3,6-dione, and explored its use in the fabrication of organic field effect transistors. In addition, we investigated its thermal, optical absorption, and electrochemical properties. Finally, the single crystal X-ray characterization is reported.

Keywords: helicenes; organic thin film transistors; Diels-Alder reaction



Citation: Bracciale, M.P.; Kwon, G.; Ho, D.; Kim, C.; Santarelli, M.L.; Marrocchi, A. Synthesis, Characterization, and Thin-Film Transistor Response of Benzo[i]pentahelicene-3,6-dione. *Molecules* **2022**, *27*, 863. <https://doi.org/10.3390/molecules27030863>

Academic Editor: Giuseppe Cirillo

Received: 30 December 2021

Accepted: 25 January 2022

Published: 27 January 2022

Publisher's Note: MDPI stays neutral with regard to jurisdictional claims in published maps and institutional affiliations.



Copyright: © 2022 by the authors. Licensee MDPI, Basel, Switzerland. This article is an open access article distributed under the terms and conditions of the Creative Commons Attribution (CC BY) license (<https://creativecommons.org/licenses/by/4.0/>).

1. Introduction

The field of organic electronics has been pushed strongly forward over recent decades, due to the synergy between different disciplines, including materials science, physics, chemistry, and engineering, as well as the interplay between academic and industrial actors [1–5].

From a synthetic chemistry point of view, significant efforts have been made to develop organic semiconducting materials, which could offer a viable alternative to their traditional inorganic counterparts. A wide range of small molecules and polymers have been successfully designed and synthesized for applications in many different devices (e.g., organic thin-film transistors (OTFTs), electrooptic modulators, organic (OPVs) or hybrid solar cells, organic light-emitting diodes (OLEDs), laser diodes, optical waveguides, and sensors), including both p-type and n-type semiconductors [6–8]. The structural diversity in terms of the core type, side chains, substituents, bridging units, conjugation extent, and shape of organic semiconductors [9–14] enables the fine-tuning of the material's properties depending on the specific device requirements.

Among the molecular materials, the possibility to create devices from organic semiconductors with a helically shaped conjugated electronic system, namely helicenes, has been gaining attention recently.

Helicenes [15–18] are inherently dissymmetric structures, made up of ortho-fused aromatic or heteroaromatic rings, in which the repulsive steric overlap of the (terminal) aromatic units and, eventually, the presence of functional groups in them determines the non-planarity of the conjugated structure, imparting a helical twist. Hence, helicenes exist in both left-handed (M, minus) and right-handed (P, plus) chiral (i.e., enantiomeric) forms.

This helically chiral, fully conjugated architecture endows these molecules with unique chiroptical properties, e.g., high optical rotatory power, strong circularly polarized luminescence, and circular dichroism [19–21].

It has been demonstrated that helicenes may be able to self-assemble into long corkscrew-shaped columns, which subsequently aggregate to form large crystalline domains in both concentrated solutions and thin films [22–25]. Besides dramatically enhancing the helicene chiroptical properties, this supramolecular aggregation may provide unique charge transport properties, as observed for, e.g., DNA [26].

Despite their peculiar properties, however, helicenes still remain rather unexplored in solid-state (opto-)electronic devices. Racemic mixtures of tetrathia-[7]-helicene [27], naphthalene double [6]helicenes [28], pyrene double [4]heterohelicene [29], 5,14-diaryldiindeno[2,1-f:1',2'-j]picene [30,31], perylene diimide double-[5]heterohelicene [32,33], and a multiple helicene containing two [5]helicene and four [4]helicene moieties [34] have been used in organic thin-film transistors (OTFTs). Some authors exploited the chirality of the helicenes by using the enantiomerically pure 1-aza[6]helicene [35] and perylene diimide double-[7]heterohelicene [36] in circularly polarized detecting OTFTs.

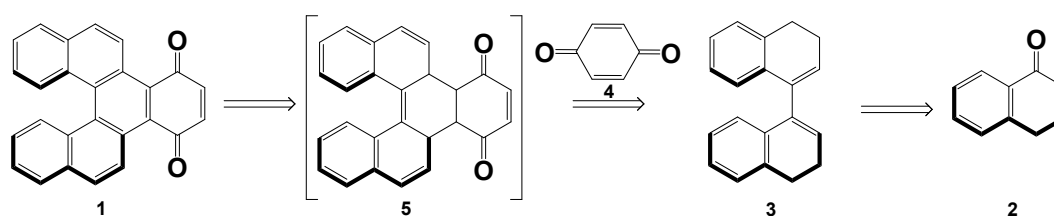
A handful of studies are available for other types of devices, such as organic light emitting diodes [37–56], organic solar cells [57–59], and hybrid DSSC [60] and perovskite solar cells [61–72].

In this paper, we report the optical, electrochemical, and structural characteristics of racemic benzo[i]pentahelicene-3,6-dione as well as its thin film, and OTFTs' semiconductor properties.

2. Results and Discussion

2.1. Synthesis

Benzo[i]pentahelicene-3,6-dione (**1**, Scheme 1) was synthesized by optimizing a previously published procedure [73]. The simplicity in this design makes this system worthy of investigation. Indeed, many advanced semiconducting helical structures are extremely challenging to access and, therefore, small quantities of material are typically available for study. Basically, the synthesis of compound **1** involves the use of α -tetralone (**2**) as a starting material, which is subjected to self-coupling in the presence of a Zn-chlorotrimethylsilane system to afford 3,3',4,4'-tetrahydro-1,1'-binaphthalene (**3**). The synthetic process was completed by the solvent-free Diels-Alder reaction of the diene **3** with ten-fold excess of 1,4-benzoquinone (**4**), followed by the in situ dehydrogenation of the resulting cycloadduct **5**. Notably, 1,4-benzoquinone, under these conditions, behaves simultaneously as a dienophile in the Diels-Alder reaction and as an oxidizing agent. Though the yield is just acceptable (~32%, see Materials and Methods), this one-step cycloaddition-dehydrogenation reaction is simple and may enable the production of the [5]helicenebenzoquinone **1** on a large scale, starting from readily available and reasonably cheap starting materials.



Scheme 1. Retrosynthesis of [5]helicenebenzoquinone **1**.

The Diels-Alder reaction represents a suitable and atom-efficient method for constructing annulated ring systems containing six-member rings [74], and it consequently offers an alternative synthetic approach to helicenes [75–84].

It is noteworthy to mention that, in our strategy, the use of excess 1,4-benzoquinone is not an issue, as the final optimized protocol also includes its recovery via steam distillation followed by filtration and reuse to minimize the waste associated with the process.

2.2. Thermal Properties

Thermal stability and transitions for [5]helicenebenzoquinone were investigated by simultaneous TGA/DSC. Representative TGA/DSC analysis curves are reported in Figure 1. As shown, the thermal decomposition takes place in two main steps until 650 °C. In the first step, the quinone loses 13.9 wt% between 30 and 341 °C. In this temperature range, the DSC curve shows an endothermic peak at 247 °C, which could be assigned to a melting point, and an exothermic peak at 295 °C due to thermal degradation or evaporation process. In addition, a continual mass loss up to 650 °C (~86.5%) associated with a broad exothermic peak, appears at 631 °C in the DSC curve. As shown, the synthesized material featured remarkable thermal stability. The onset point of the weight loss with 5% weight loss temperature (decomposition temperature T_d) was 268 °C, and no weight loss was observed at lower temperatures.

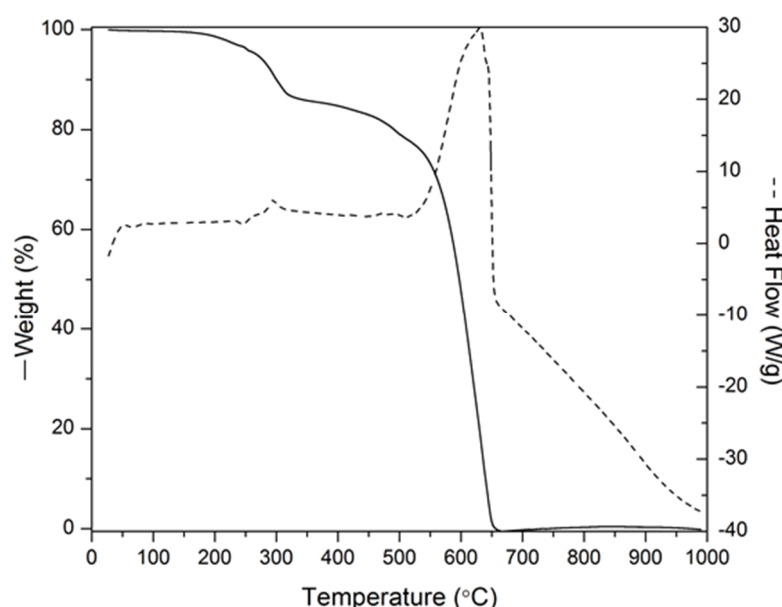


Figure 1. TGA (solid line) and DSC (dotted line) thermograms of the [5]helicenebenzoquinone (exotherm up).

2.3. Optical and Electrochemical Properties

The solution and thin-film photophysical properties of the synthesized quinone were assessed by optical absorption (ultraviolet-visible (UV-vis)) spectroscopy, and cyclic voltammetry (CV) was used to identify its electrochemical behavior.

Cyclic voltammogram and absorbance spectra of the compound are shown in Figure 2, and electrochemical and optical data are summarized in Table 1.

Table 1. Thermal, electrochemical and spectroscopic characterization of [5]helicenebenzoquinone 1.

m.p (°C)	$E_{1/2-ox}$ (V)	$E_{1/2-red}$ (V)	$\lambda_{max-sol}$ (nm) ^a	ϵ ($Lmol^{-1}cm^{-1}$)	E_{g-sol} (eV) ^a	$\lambda_{max-film}$ (nm) ^b	E_{g-film} (eV) ^b	LUMO (eV) ^c	HOMO (eV) ^d
246	-	-1.67	486	$8.33 \cdot 10^3$	2.11	490	2.01	-3.14	-5.25

^a Optical band gap estimated from the low-energy band edge in the optical spectrum. Concentrations are 10^{-4} – 10^{-5} M in $CHCl_3$; ^b Optical bandgap estimated from absorption onset ($E_g = 1240/\lambda_{onset}$) of spin-cast film from 5 mg/mL of $CHCl_3$ solution on glass substrates; ^c $E_{LUMO} = [-(E_{red} - E_{1/2-ferrocene}) + 4.8]$; ^d $E_{HOMO} = E_{LUMO} - E_{opt.gap}$.

Optical absorption and emission maxima were performed in solution and as thin films on glass substrates (Figure 2a).

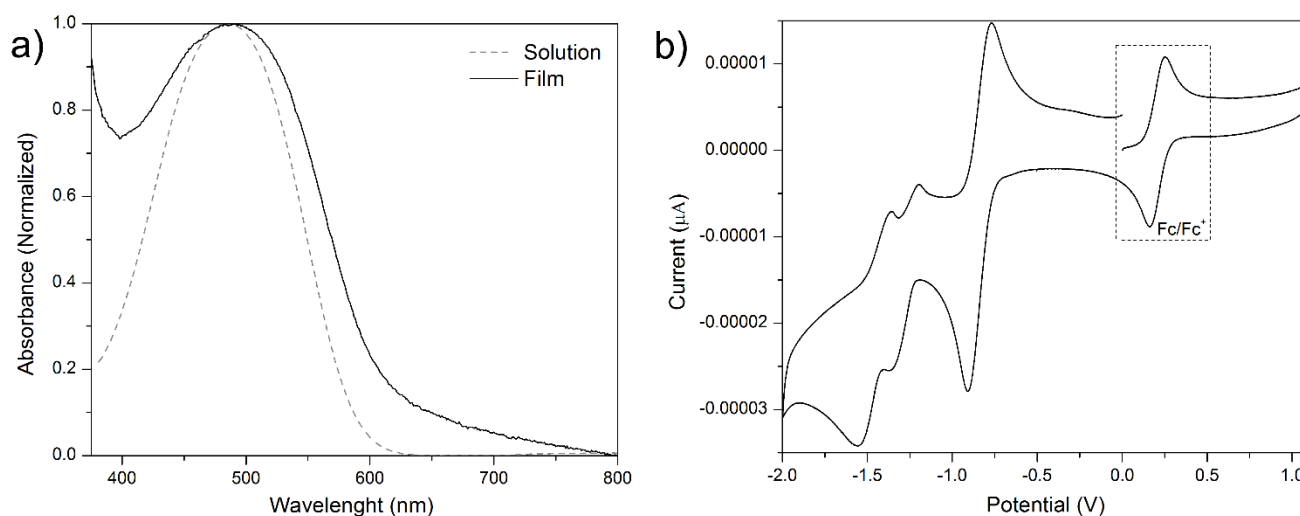


Figure 2. (a) UV-vis normalized absorptions of [5]helicenebenzoquinone in solution (CHCl_3) and as a thin film; (b) cyclic voltammetry; 10^{-3} M CH_2Cl_2 , 0.1 M NBu_4PF_6 , $T = 25^\circ\text{C}$, scan rate: 100 mVs^{-1} , reference electrode: Ag/AgCl , working electrode: glassy carbon. Fc/Fc^+ was used as internal reference ($E_{1/2}\text{-ferrocene} = 0.21\text{ V}$).

In chloroform (CHCl_3), the studied quinone exhibits an absorption maximum ($\lambda_{\text{max-sol}}$) located at 486 nm and a molar extinction coefficient (ϵ) of $8.33 \times 10^3\text{ Lmol}^{-1}\text{cm}^{-1}$.

A thin film of the same compound shows a sizeable broadening and exhibits an absorption maximum ($\lambda_{\text{max-film}}$) at 490 nm. The broadening and the small bathochromic shift ($<10\text{ nm}$), observed going from the solution to the thin film, is clear evidence of solid-state J-aggregate formation [85,86]. Interestingly, a tail in the [5]helicene film absorption profile can be observed, spanning from 600 to 800 nm. This might have a component [87] from spatially proximal interactions between the dipole–dipole interactions of the quinone fragment, facilitated by the tendency of the helicene molecules to self-assemble, that can modulate the spectral transition above 600 nm and create a tail in the absorption spectrum.

The band gap for the [5]helicene **1** was estimated from the low-energy band edges (Table 1). The optical band gaps of the compound in solution and solid state are estimated to be 2.11 and 2.01 eV, respectively.

The CV plot (Figure 2b) show the presence of a reversible reduction process with half-wave potentials at -1.46 V . No oxidation peaks are observed in the investigated electrochemical window.

From the reduction potential, LUMO and HOMO energies were estimated knowing that the SCE energy level is -4.8 eV below the vacuum level and the band gap obtained by optical absorption data ($E_{\text{g-sol}}$) (Table 1), respectively. Using these relations, the LUMO value was estimated to lie at -3.14 eV , and HOMO was calculated as -5.25 eV .

2.4. Quantum Mechanical Calculations

To gain an insight into the electronic properties of [5]helicenebenzoquinone, quantum-chemical calculations were also performed. The optimized geometry, molecular orbitals' contour plots (MO), and energy diagram are shown in Figure 3.

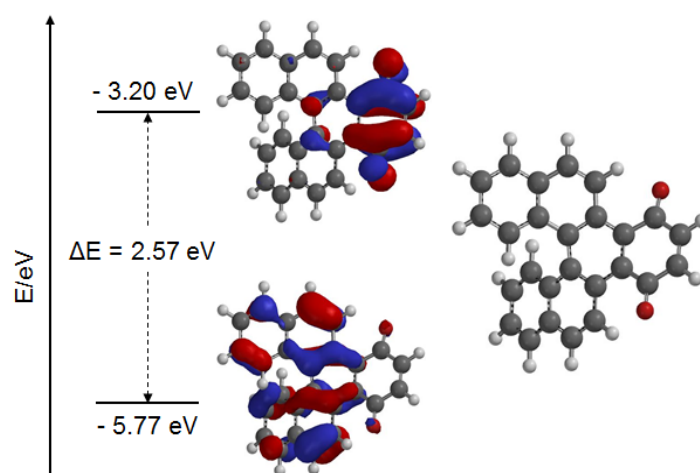


Figure 3. Computational (DFT) values of HOMO/LUMO/gap energies, MO electron density contours and structure of [5]helicenebenzoquinone.

The molecular orbital (MO) energies and contours were calculated by using the DFT-optimized structure of the molecule [79]. Since charge is transported through the frontier molecular orbitals of organic semiconductors, their geometries, energies, and extents of delocalization directly affect carrier stability and intermolecular hopping rates. Ideally, the HOMO and LUMO are delocalized over the entire π -core of the semiconductor for p- and n-channel transport, respectively [86].

Here, the HOMO is delocalized over the ortho-anellated moiety, while the LUMO is more compact, since it is delocalized only on the benzoquinone subunit. This highly localized nature of the LUMO limits intermolecular π -overlap and may favor charge trapping at the quinone site. This may be a contributing factor to the limited mobility values of [5]helicenebenzoquinone (*vide infra*). This is not uncommon behavior [88] for quinone-containing semiconductors. The computed HOMO energy is -5.77 eV, while the LUMO energy is -3.20 eV.

The DFT-calculated HOMO and LUMO energies are in good agreement with the experimental values (Figure 3 and Table 1, respectively).

2.5. Crystallographic Characterization

The X-ray analysis was carried out on a recrystallized single crystal obtained from [5]helicenebenzoquinone solution. The crystal data and structure refinement are reported in Tables 2 and S1–S6 (Supplementary Information).

Table 2. Summary of crystal data and structure refinement.

Parameter	Data
Empirical Formula	$C_{26}H_{14}O_2$
Formula weight	358.37
Temperature/ $^{\circ}C$	-173.16
Crystal system	Orthorhombic
Space group	Pbca (no. 61)
a / \AA , b / \AA , c / \AA	12.1651 (3), 7.4140 (2), 36.6996 (7)
$\alpha /^{\circ}$, $\beta /^{\circ}$, $\gamma /^{\circ}$	90, 90, 90
Volume / \AA^3	3310.01 (14)

Table 2. Cont.

Parameter	Data
Z	8
$\rho_{\text{calc}}/\text{mg mm}^{-3}$	1.438
$\mu(\text{MoK}\alpha)/\text{mm}^{-1}$	0.090
F (000)	1488
Crystal size/ mm^3	$0.24 \times 0.15 \times 0.069$
2 θ range for data collection	5.562 to 56.558°
Index ranges	$-15 \leq h \leq 16, -9 \leq k \leq 9, -48 \leq l \leq 48$
Reflections collected	55,869
Independent reflections	4094 [R(int) = 0.1036]
Data/restraints/parameters	4094/0/253
Goodness-of-fit on F^2	1.035
Final R indexes [$I > 2\sigma(I)$]	$R_1 = 0.0459, wR_2 = 0.1030$
Final R indexes [all data]	$R_1 = 0.0698, wR_2 = 0.1151$
Largest diff. peak/hole/ $e \text{ \AA}^{-3}$	0.301/−0.228

2.6. Thin-Film Transistor Characterization

Top-contact OTFTs (1000 μm channel widths (W) and 50 μm channel lengths (L)) were fabricated by spin coating or drop casting films on 300 nm SiO_2 (Bare), poly-4-vinylphenol (PVP) and PS-brush (PS-OH)-treated SiO_2 substrates. The current–voltage characteristics of the fabricated organic thin film transistor (OTFT) devices were measured at room temperature and the device performance (mobility, current on/off ratio, and threshold voltage) data and representative output and transfer curves are reported in Table 3 and Figure 4, respectively. The field-effect carrier mobility (μ) of the semiconductor was calculated in the saturation regime using the conventional transistors relationship: $\mu_{\text{sat}} = (2I_{\text{DS}}L)/[WC_{\text{ox}}(V_{\text{sg}} - V_{\text{th}})^2]$, where I_{sd} is the source-drain saturation current; C_{ox} is the areal capacitance value of the insulator layer, V_{sg} is the gate voltage, and V_{th} is the threshold voltage. The latter can be estimated as the x intercept of the linear section of the plot of V_{sg} vs. $(I_{\text{sd}})^{1/2}$.

Table 3. Hole mobilities ($\text{cm}^2/\text{V}^{-1}\text{s}^{-1}$), current on/off ratios ($I_{\text{on}}/I_{\text{off}}$), and threshold voltages (V_{T} , V) for films deposited at various substrates, substrate temperatures (T_{D} , °C) and annealing temperatures (T_{A} , °C); nw: not working.

Substrate	Solvent	T_{D}	T_{A}	μ_{h}	$I_{\text{on}}/I_{\text{off}}$	V_{T}
Spin-Coated (SC)						
Bare	chlorobenzene	-	-	1.6×10^{-5}	1.5×10^3	1.5
Bare	dichlorobenzene	-	150		nw	
Bare	Toluene	-	150		nw	
PVP	dichlorobenzene	-	150		nw	
PVP	Toluene	-	150		nw	
PS brush	dichlorobenzene	-	150		nw	
PS brush	Toluene	-	150		nw	
Drop-casted (DC)						
Bare	chlorobenzene	100	130	1.5×10^{-7}	3.0×10^4	−23
PVP	chlorobenzene	100	130	5.3×10^{-5}	6.0×10^3	−10
PS brush	dichlorobenzene	60	150	6.0×10^{-5}	3.0×10^3	−67
PS brush	chlorobenzene	70	-	2.5×10^{-6}	5.0×10^3	−35
PS brush	chlorobenzene	70	150	4.8×10^{-5}	2.5×10^4	−23

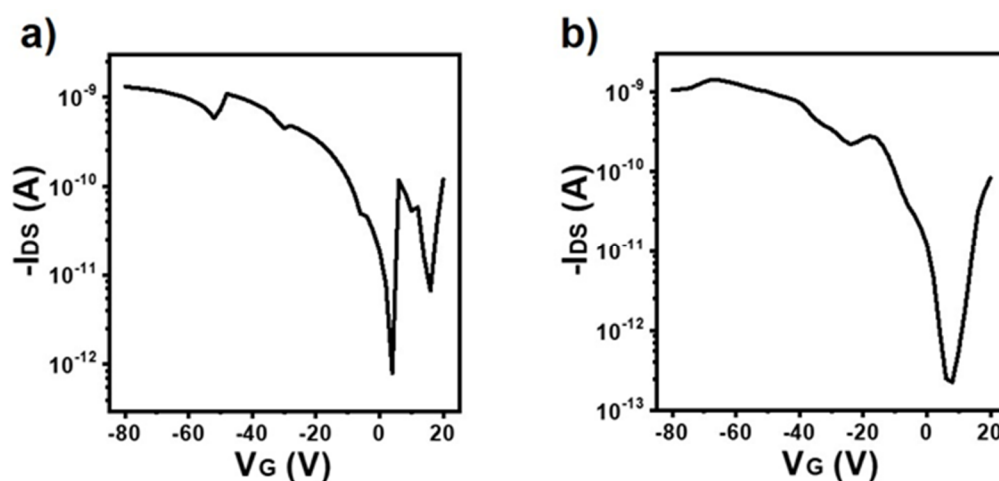


Figure 4. Transfer plot of the OTFT device obtained via (a) the SC method onto bare SiO₂ (not annealed), and (b) the DC method onto the PS brush with annealing treatment (150 °C).

[5]Helicenebenzoquinone showed a p-type behavior, with hole mobilities of 10^{-5} – 10^{-7} cm²/Vs and current on/off ratio of 10^3 – 10^4 .

The device response was found to be dependent on both the deposition method (SC or DC) and the dielectric surface treatment. Both have a critical impact on the π – π stacking and intermolecular interaction between the semiconductor molecules and influence the neighbouring molecular orbital overlapping. In the case of SC, although the uniformity of the thin film is generally excellent, there is a disadvantage of low crystallinity. On the other hand, DC generally results in highly crystalline thin films, whereas the uniformity is poor. Overall, devices fabricated by DC deposition performed better than the spin-coated counterparts. By comparing the performance of the SC and DC devices in Table 3, it can be implied that the slow, static process of DC facilitates preferable ordering of the [5]helicenebenzoquinone molecules compared to the SC method. The majority of the non-working and poor SC devices may be at least in part be attributed to the poor molecular ordering due to the accelerated solvent evaporation from spin-coating.

Among the devices obtained by the DC method, those on the PS brush demonstrated the best results. PS brush treatment is a widely used surface modification method which optimizes the morphology, surface energy, and viscoelastic properties of the resulting dielectrics [89]. The modification of the semiconductor/dielectric interface is crucial to the growth of the semiconductor layer, which leads to enhanced OTFT characteristics.

Representative micrographies of the thin films are reported in Figure S1 (Supplementary Information). It can be observed that in all cases they typically show gaps between (inhomogeneous) crystallites, which likely contribute to compromising charge transport. No evident correlation between T_D and device performance could be identified.

3. Materials and Methods

All chemicals were purchased from Merck KGaA, Darmstadt, Germany, and used without further purification unless otherwise noted. Column chromatography was performed on silica gel (230–400 mesh American Society for Testing and Materials, ASTM) as a stationary phase. 3,3',4,4'-tetrahydro-1,1'-binaphthalene (**2**) was prepared according to a previously reported procedure [73].

NMR spectra were recorded on a Varian Associates (Palo Alto, CA, USA) VXR-400 multinuclear spectrometer using deuterated chloroform (CDCl₃) as the solvent (internal Me₄Si). Elemental microanalyses were performed using a Fisons' (Ipswich, London, UK) EA1106 CHN analyzer using atropine (C₁₇H₂₃NO₃), 2,5-bis-2-(5-tertbutylbenzoxazol-yl)-thiophene (C₂₆H₂₆N₂O₂S; BBOT) and phenanthrene (C₁₄H₁₀) as a reference standard, with an accuracy of ≈ 2 μ mol g⁻¹. The melting point was measured on a Büchi 510 instrument (Büchi Labortechnik AG, Flawil, CH) and was not corrected. Thermogravimetric (TGA)

and differential scanning calorimetric (DSC) analyses were performed on a TGA/DSC simultaneous apparatus (SDT Q600, TA Instruments, New Castle, Delaware, UK) under a nitrogen flow rate of 100 mL min^{-1} . Samples in an open platinum cell were heated from 30 up to $1000 \text{ }^\circ\text{C}$ with a rate of $10 \text{ }^\circ\text{C min}^{-1}$. Absorption spectra of the compound in chloroform (CHCl_3) were recorded using a Varian Cary 100 UV-vis spectrophotometer (using a glass cuvette of 1 cm path length) over the spectral range of 350–800 nm. Electrochemical properties were determined using a Bass potentiostat, with a conventional three-electrode configuration (platinum-wire counter electrode, glassy carbon working electrode, and silver/silver chloride (Ag/AgCl) reference electrode). Cyclic voltammetry was performed in an electrolyte solution of 0.1 M tetrabutylammonium hexafluorophosphate ($\text{C}_{16}\text{H}_{36}\text{F}_6\text{NP}$; TBAPF₆) in dichloromethane (CH_2Cl_2 ; DCM) with scan rates between 50 and 100 mVs^{-1} . The solutions were purged with nitrogen steam for about 15 min before every experiment. The glassy carbon working electrode was polished with a slurry of alumina and ultrapure water on a Buehler felt pad and rinsed thoroughly with ultrapure water. A ferrocene/ferrocenium redox (Fc/Fc⁺) couple was used as an internal standard. The HOMO and LUMO energy levels were calculated from the oxidation (E_{ox}) and reduction (E_{red}) potentials data using the empirical relation $E_{\text{LUMO}} = [-(E_{\text{red}} - E_{1/2\text{-ferrocene}}) + 4.8] \text{ eV}$ or $E_{\text{HOMO}} = [-(E_{\text{ox}} - E_{1/2\text{-ferrocene}}) + 4.8] \text{ eV}$. Density functional theory (DFT) computations were carried out using the Spartan '08 software package (Wavefunction, Inc., Irvine, CA, USA) at the B3LYP/6-31G* level. Single crystals of helicene were recrystallized by layering chloroform (CHCl_3) solution of the synthesized material with hexane (C_6H_{14}). Suitable crystals were mounted in inert oil and transferred to the cold gas stream of a Bruker (Billerica, MA, USA) Kappa APEX CCD area detector equipped with a MoK α sealed tube with graphite. The crystal was kept at $-173.16 \text{ }^\circ\text{C}$ during data collection. SADABS-2012/1 (Bruker) was used for absorption correction. Using Olex2 [90], the structure was solved with the XT structure solution program using direct methods and refined with the ShelXL [91] refinement package using least squares minimization.

3.1. Diels-Alder Reaction of 3,3',4,4'-Tetrahydro-1,1'-binaphthalene (3) with 1,4-Benzoquinone (4)

The diene 3 (5.2 g, 19.9 mmol) and 1,4-benzoquinone (4) (22 g, 0.2 mol) were heated together at $150\text{--}170 \text{ }^\circ\text{C}$ for 18 h in a degassed flask. The excess benzoquinone was removed by steam distillation from the crude reaction mixture, and the residue was purified by column chromatography (silica gel, hexane/ethylacetate 3:1) to afford benzo[i]pentahelicene-3,6-dione (1). Yield: 32%; m.p. $246\text{--}247 \text{ }^\circ\text{C}$. The spectra matched those in the literature. $^1\text{H-NMR}$ (CDCl_3) δ 6.97 (s, 1H), 7.21 (dd, 1H, $J = 8.6, 7.0 \text{ Hz}$), 7.54 (dd, 1H, $J = 8.1, 7.0 \text{ Hz}$), 7.92 (d, 1H, $J = 8.1 \text{ Hz}$), 8.04 (d, 1H, $J = 9.2 \text{ Hz}$), 8.13 (d, 1H, $J = 8.6 \text{ Hz}$), 9.24 (d, 1H, $J = 9.2 \text{ Hz}$). An. Calcd. for $\text{C}_{26}\text{H}_{14}\text{O}_2$: C%, 87.13; H%, 3.94. Found: C%, 87.30; H%, 3.96.

3.2. OTFTs Fabrication and Characterization

Bottom-gate/top-contact organic thin-film transistors (OTFTs) were fabricated on heavily n-doped (100) silicon substrate (resistivity $< 0.005 \text{ } \Omega\text{cm}$) with a thermally grown silicon dioxide (300 nm SiO_2) as the dielectric layer. Prior to deposition, the Si/ SiO_2 substrate were cleaned in an ultrasonic bath using acetone ($\text{C}_3\text{H}_8\text{O}$) for 15 min, dried using a nitrogen gun, and cleaned with air plasma for 5 min (Harrick Plasma, Ithaca, NY, USA18 W). In order to reduce charge trapping and thus enhance mobility, the SiO_2 substrate was modified with poly-4-vinylphenol ($(\text{C}_8\text{H}_8\text{O})_n$; PVP) or PS-brush ($(\text{CH}_2\text{CH}(\text{C}_6\text{H}_5))_n\text{OH}$; PS-OH). Semiconducting layers were deposited via two different solution-processing methods: spin-coating (SC) and drop-casting (DC). For the SC process, the pentahelicenebenzoquinone was dissolved in chlorobenzene ($\text{C}_6\text{H}_5\text{Cl}$), dichlorobenzene ($\text{C}_6\text{H}_4\text{Cl}_2$), or toluene (C_7H_8), and the solutions (15 mg/mL) were spin-coated at 3000 rpm for 30 s onto the substrates. The substrates were annealed at $150 \text{ }^\circ\text{C}$ under vacuum overnight. For the DC process, a 0.2 wt% solution of semiconductor in chlorobenzene ($\text{C}_6\text{H}_5\text{Cl}$) was deposited onto the substrates heated at 100 and $60\text{--}70 \text{ }^\circ\text{C}$ for bare, PS-brush- and PVP-treated substrates, respectively. The substrates were then annealed at $130\text{--}150 \text{ }^\circ\text{C}$ for 5 h under vacuum. Top contacts were

fabricated by vapor deposition of gold electrodes ($\sim 10^{-6}$ Torr, 0.2 \AA s^{-1} , ~ 40 nm thick) onto the semiconductor thin films through a shadow mask to obtain devices with a channel width (W) and length (L) of 1000 and 50 μm , respectively. The capacitance of the 300 nm SiO_2 gate insulator was 11.4 nFcm^{-2} . Characterization of the devices was performed at room temperature in ambient atmosphere using a Keithley 4200 SCS (Keithley Instruments, Cleveland, OH, USA).

4. Conclusions

A helicene quinone, namely benzo[i]pentahelicene-3,6-dione, was prepared in one-pot reaction conditions via Diels–Alder cycloaddition-dehydrogenation steps. Its thermal, optical, and electrochemical behavior, along with its single-crystal structure and electronic structure, were also reported. [5]Helicenebenzoquinone exhibited excellent thermal stability, and near UV-vis electronic absorption.

An OTFT that incorporated the helical compound as a semiconductor with the configuration of bottom-gate/top-contact attained hole mobilities in the range of 10^{-5} – $10^{-7} \text{ cm}^2/\text{Vs}$ and current on/off ratio of 103–104 was formulated. The carrier mobilities were found to depend on the thin-film deposition method, and surface treatments.

This study contributes to gaining insights into the structure–properties–device response relationship in the class of helically shaped semiconducting materials. The strongly localized LUMO may be at least partially responsible for the limited mobility values of [5]helicenebenzoquinone. The tendency to form J-aggregates (i.e., less orbital overlap) and the presence of significant gaps between (heterogeneous) crystallites in thin-films also possibly compromise charge transport.

On the other hand, the LUMO localization and the J-aggregation, along with the excellent thermal stability, suggest the use of [5]helicenequinone in OLED devices with thermally activated delayed fluorescence (TADF) emitters [92].

Hence, future developments will be focused on expanding the range of device applications, including organic–inorganic hybrids. This is also worth pursuing in view of the fact that the optimized synthetic method enables us to prepare the [5]helicenebenzoquinone on a large scale, which is a key requirement for studying organics' applications as materials for electronics. In addition, its structural simplicity, compared with other advanced double or multiple helicenes, is a design principle that can be applied in the development of semiconductors, to make the leap beyond the laboratory scale.

New helical architectures will be realized by introducing, e.g., substituents at the terminal aromatic rings, to tune the helical twisting of the structure, which can ultimately result in unique stacking structures.

Their optical resolution into enantiomerically pure forms will be also pursued.

Supplementary Materials: The following supporting information can be downloaded online, Figure S1: Microscopic view of thin films obtained by (a) SC from chlorobenzene onto bare SiO_2 (not annealed); (b) SC from dichlorobenzene onto bare SiO_2 (annealed at $150 \text{ }^\circ\text{C}$); (c) SC from dichlorobenzene onto bare PVP (annealed at $150 \text{ }^\circ\text{C}$); (d) DC from chlorobenzene onto bare SiO_2 (annealed at $130 \text{ }^\circ\text{C}$; $T_D = 100 \text{ }^\circ\text{C}$) and (e) onto PS brush (annealed at $150 \text{ }^\circ\text{C}$; $T_D = 70 \text{ }^\circ\text{C}$); Table S1: Fractional Atomic Coordinates ($\times 10^4$) and Equivalent Isotropic Displacement Parameters ($\text{\AA}^2 \times 10^3$) for compound **1**; Table S2: Anisotropic Displacement Parameters ($\text{\AA}^2 \times 10^3$) for compound **1**; Table S3: Bond Lengths for compound **1**; Table S4: Bond Angles for compound **1**; Table S5: Torsion Angles for compound **1**; Table S6: Hydrogen Atom Coordinates ($\text{\AA} \times 10^4$) and Isotropic Displacement Parameters ($\text{\AA}^2 \times 10^3$) for compound **1**.

Author Contributions: Conceptualization, M.P.B. and A.M.; methodology, M.P.B., C.K. and A.M.; literature survey, A.M., M.P.B., C.K., M.L.S. and A.M.; investigation, A.M., G.K. and D.H.; writing—original draft preparation, M.P.B., C.K. and A.M.; writing—review and editing, M.P.B., M.L.S. and A.M.; supervision, M.P.B., C.K. and A.M. All authors have read and agreed to the published version of the manuscript.

Funding: This research was partially funded by “Fondo Ricerca di Base” 2019, University of Perugia, Perugia, Italy.

Institutional Review Board Statement: Not applicable.

Informed Consent Statement: Not applicable.

Conflicts of Interest: The authors declare no conflict of interest.

Sample Availability: Samples of the compounds are not available from the authors.

References

1. Liao, C.-Y.; Chen, Y.; Lee, C.-C.; Wang, G.; Teng, N.-W.; Lee, C.-H.; Li, W.-L.; Chen, Y.-K.; Li, C.-H.; Ho, H.-L.; et al. Processing strategies for an organic photovoltaic module with over 10% efficiency. *Joule* **2020**, *4*, 189–206. [CrossRef]
2. Cui, Y.; Yao, H.; Zhang, J.; Xian, K.; Zhang, T.; Hong, L.; Wang, Y.; Xu, Y.; Ma, K.; An, C.; et al. Single-junction organic photovoltaic cells with approaching 18% efficiency. *Adv. Mater.* **2020**, *32*, 1908205. [CrossRef] [PubMed]
3. PV Magazine. An Organic Solar Cell with 25% Efficiency. 2020. Available online: <https://www.pv-magazine.com/2020/03/24/an-organic-solar-cell-with-25-efficiency/> (accessed on 29 December 2021).
4. Acharya, R.; Peng, B.; Chan, P.K.L.; Schmitz, G.; Klauk, H. Achieving ultralow turn-on voltages in organic thin-film transistors: Investigating fluoroalkylphosphonic acid self-assembled monolayer hybrid dielectrics. *ACS Appl. Mater. Interfaces* **2019**, *11*, 27104–27111. [CrossRef] [PubMed]
5. Hosono, H.; Kim, J.; Toda, Y.; Kamiya, T.; Watanabe, S. Transparent amorphous oxide semiconductors for organic electronics: Application to inverted OLEDs. *Proc. Natl. Acad. Sci. USA* **2016**. [CrossRef] [PubMed]
6. Mishra, A.; Bäuerle, P. Small molecule organic semiconductors on the move: Promises for future solar energy technology. *Angew. Chem. Int. Ed.* **2012**, *51*, 2020–2067. [CrossRef] [PubMed]
7. Pankow, R.M.; Thompson, B.C. The development of conjugated polymers as the cornerstone of Organic electronics. *Polymer* **2020**, *207*, 122874. [CrossRef]
8. Sun, H.; Guo, X.; Facchetti, A. High-performance n-type polymer semiconductors: Applications, recent development, and challenges. *Chem* **2020**, *6*, 1310–1326. [CrossRef]
9. Cheng, P.; Yang, Y. Narrowing the band gap: The key to high-performance organic photovoltaics. *Acc. Chem. Res.* **2020**, *53*, 1218–1228. [CrossRef]
10. Facchetti, A. π -Conjugated Polymers for Organic Electronics and Photovoltaic Cell Applications. *Chem. Mater.* **2011**, *23*, 733–758. [CrossRef]
11. Seri, M.; Marrocchi, A. The carbon-carbon triple bond as a tool to design organic semiconductors for photovoltaic applications: An assessment of prospects and challenges. *J. Mater. Chem C* **2021**, *9*, 16164–16186. [CrossRef]
12. Seri, M.; Marrocchi, A.; Bagnis, D.; Ponce, R.; Taticchi, A.; Marks, T.J.; Facchetti, A. Molecular shape-controlled photovoltaic performance probed via soluble pi-conjugated arylacetylenic semiconductors. *Adv. Mater.* **2011**, *23*, 3827–3831. [PubMed]
13. Bagnis, D.; Beverina, L.; Huang, H.; Silvestri, F.; Yao, Y.; Yan, H.; Pagani, G.A.; Marks, T.J.; Facchetti, A. Marked alkyl-vs alkenyl-substituent effects on squaraine dye solid-state structure, carrier mobility, and bulk-heterojunction solar cell efficiency. *J. Am. Chem. Soc.* **2010**, *132*, 4074–4075. [CrossRef]
14. Broggi, A.; Tomasi, I.; Bianchi, L.; Marrocchi, A.; Vaccaro, L. Small molecular aryl acetylenes: Chemically tailoring high-efficiency organic semiconductors for solar cells and field-effect transistors. *ChemPlusChem* **2014**, *79*, 486–507. [CrossRef] [PubMed]
15. Shen, Y.; Chen, C.F. Helicenes: Synthesis and applications. *Chem. Rev.* **2012**, *112*, 1463–1535. [CrossRef] [PubMed]
16. Martin, R.H. The Helicenes. *Angew. Chem. Int. Ed. Engl.* **1974**, *13*, 649–660. [CrossRef]
17. Laarhoven, W.H.; Prinsen, W.J.C. Carbohelicenes and Heterohelicenes. *Top. Curr. Chem.* **1984**, *125*, 63–130.
18. Meurer, K.P.; Vögtle, F. Helical Molecules in Organic Chemistry. *Top. Curr. Chem.* **1985**, *127*, 1–76.
19. Mori, T. Chiroptical Properties of Symmetric Double, Triple, and Multiple Helicenes. *Chem. Rev.* **2021**, *121*, 2373–2412. [CrossRef]
20. Grimme, S.; Harren, J.; Sobanski, A.; Vögtle, F. Structure/Chiroptics Relationships of Planar Chiral and Helical Molecules. *Eur. J. Org. Chem.* **1998**, *1998*, 1491–1509. [CrossRef]
21. Groen, M.B.; Wynberg, H. Optical Properties of Some Heterohelicenes. Absolute Configuration. *J. Am. Chem. Soc.* **1971**, *93*, 2968–2974. [CrossRef]
22. Verbiest, T.; Elshocht, S.V.; Kauranen, M.; Hellemans, L.; Snauwaert, J.; Nuckolls, C.; Katz, T.J.; Persoons, A. Strong enhancement of nonlinear optical properties through supramolecular chirality. *Science* **1998**, *282*, 913–915. [CrossRef] [PubMed]
23. Nuckolls, C.; Katz, T.J.; Castellanos, L. Aggregation of conjugated helical molecules. *J. Am. Chem. Soc.* **1996**, *118*, 3767–3768. [CrossRef]
24. Rybáček, J.; Stará, I.G.; Starý, I.; Rahe, P.; Nimmrich, M.; Kühnle, A. Racemic and Optically Pure Heptahelicene-2-carboxylic Acid: Its Synthesis and Self-Assembly into Nanowire-Like Aggregates. *Eur. J. Org. Chem.* **2011**, 853–860. [CrossRef]
25. Katz, T.J. Syntheses of Functionalized and Aggregating Helical Conjugated Molecules. *Angew. Chem. Int. Ed.* **2000**, *39*, 1921–1923. [CrossRef]
26. Lewis, F.D.; Liu, X.; Wu, Y.; Zuo, X. DNA-Mediated Exciton Coupling and Electron Transfer between Donor and Acceptor Stilbenes Separated by a Variable Number of Base Pairs. *J. Am. Chem. Soc.* **2003**, *125*, 12729. [CrossRef]

27. Kim, C.; Marks, T.J.; Facchetti, A.; Schiavo, M.; Bossi, A.; Maiorana, S.; Licandro, E.; Todescato, F.; Toffanin, S.; Muccini, M.; et al. Synthesis, characterization, and transistor response of tetrathia-[7]-helicene precursors and derivatives. *Org. Electron.* **2009**, *10*, 1511–1520. [[CrossRef](#)]
28. Fujikawa, T.; Mitoma, N.; Wakamiya, A.; Saeki, A.; Segawa, Y.; Itami, K. Synthesis, properties, and crystal structures of π -extended double [6]helicenes: Contorted multi-dimensional stacking lattice. *Org. Biomol. Chem.* **2017**, *15*, 4697–4703. [[CrossRef](#)]
29. Moriguchi, T.; Higashi, M.; Yakeya, D.; Jalli, V.; Tsuge, A.; Okauchi, T.; Nagamatsu, S.; Takashima, W. Synthesis, characterization and air stable semiconductor properties of thiophene-condensed pyrene derivatives. *J. Mol. Struct.* **2017**, *1127*, 413–418. [[CrossRef](#)]
30. Hsieh, Y.-C.; Wu, C.F.; Chen, Y.-T.; Fang, C.-T.; Wang, C.-S.; Li, C.-H.; Chen, L.-Y.; Cheng, M.-J.; Chueh, C.-C.; Chou, P.-T.; et al. 5,14-Diaryldiindeno[2,1-f:1',2'-j]picene: A New Stable [7] Helicene with a Partial Biradical Character. *J. Am. Chem. Soc.* **2018**, *140*, 14357–14366. [[CrossRef](#)]
31. Shen, S.-W.; Chen, D.G.; Chen, I.-T.; Chang, K.H.; Lee, C.-W.; Fang, C.T.; Chen, Y.T.; Chuang, W.T.; Lee, Y.H.; Wu, Y.T.; et al. Delayed Charge Recombination by Open-Shell Organics: Its Application in Achieving Superb Photodetectors with Broadband (400–1160 nm) Ultrahigh Sensitivity and Stability. *Adv. Opt. Mater.* **2020**, *8*, 1902179. [[CrossRef](#)]
32. Schaack, C.; Evans, A.M.; Ng, F.; Steigerwald, M.L.; Nuckolls, C. High-Performance Organic Electronic Materials by Contorting Perylene Diimides. *J. Am. Chem. Soc.* **2021**, *144*, 42–51. [[CrossRef](#)] [[PubMed](#)]
33. Zeng, C.; Xiao, C.; Feng, X.; Zhang, L.; Jiang, W.; Wang, Z. Electron-Transporting Bis (heterotetracenes) with Tunable Helical Packing. *Angew. Chem. Int. Ed.* **2018**, *57*, 10933. [[CrossRef](#)] [[PubMed](#)]
34. Yang, Y.; Yuan, L.; Shan, B.; Liu, Z.; Miao, Q. Twisted Polycyclic Arenes from Tetranaphthylidiphenylbenzenes by Controlling the Scholl Reaction with Substituents. *Chem. Eur. J.* **2016**, *22*, 18620. [[CrossRef](#)] [[PubMed](#)]
35. Yang, Y.; Correa da Costa, R.; Fuchter, M.J.; Campbell, A.J. Circularly polarized light detection by a chiral organic semiconductor transistor. *Nat. Photonics* **2013**, *7*, 634–638. [[CrossRef](#)]
36. Zhang, L.; Song, I.; Ahn, J.; Han, M.; Linares, M.; Surin, M.; Zhang, H.-J.; Oh, J.H.; Lin, J. π -Extended perylene diimide double-heterohelicenes as ambipolar organic semiconductors for broadband circularly polarized light detection. *Nat. Commun.* **2021**, *12*, 142. [[CrossRef](#)]
37. Oda, S.; Kawakami, B.; Yamasaki, Y.; Matsumoto, R.; Yoshioka, M.; Fukushima, D.; Nakatsuka, S.; Hatakeyama, T. One-Shot Synthesis of Expanded Heterohelicene Exhibiting Narrowband Thermally Activated Delayed Fluorescence. *J. Am. Chem. Soc.* **2021**. [[CrossRef](#)]
38. Shi, Y.; Yang, G.; Shen, B.; Yang, Y.; Yan, L.; Yang, F.; Liu, J.; Liao, X.; Yu, P.; Bin, Z.; et al. Insight into Regioselective Control in Aerobic Oxidative C-H/C-H Coupling for C3-Arylation of Benzothiophenes: Toward Structurally Nontraditional OLED Materials. *J. Am. Chem. Soc.* **2021**, *143*, 21066–21076. [[CrossRef](#)]
39. Li, M.; Wang, Y.-F.; Zhang, D.-W.; Zhang, D.; Hu, Z.-Q.; Duan, L.; Chen, C.-F. Thermally activated delayed fluorescence material-sensitized helicene enantiomer-based OLEDs: A new strategy for improving the efficiency of circularly polarized electroluminescence. *Sci. China Chem.* **2021**, *64*, 899–908. [[CrossRef](#)]
40. Dhbaibi, K.; Abella, L.; Meunier-Della-Gatta, S.; Roisnel, T.; Vanhuyne, N.; Jamoussi, B.; Pieters, G.; Racine, B.; Quesnel, E.; Autschbach, J.; et al. Achieving high circularly polarized luminescence with push-pull helicenic systems: From rationalized design to top-emission CP-OLED applications. *Chem. Sci.* **2021**, *12*, 5522–5533. [[CrossRef](#)]
41. Ikari, Y.; Kaihara, T.; Goto, S.; Bovenkerk, M.; Grenz, D.C.; Esser, B.; Ferreira, M.; Stachelek, P.; Data, P.; Yoshida, T.; et al. Peripherally Donor-Installed 7,8-Diaza[5]helicenes as a Platform for Helical Luminophores. *Synthesis* **2021**, *53*, 1584–1596.
42. Yan, Z.-P.; Luo, X.-F.; Liao, K.; Zheng, Y.-X.; Zuo, J.-L. Rational design of the platinahelicene enantiomers for deep-red circularly polarized organic light-emitting diodes. *Front. Chem.* **2020**, *8*, 501. [[CrossRef](#)] [[PubMed](#)]
43. Zhao, Y.; Ding, J.; Han, X.; Geng, T.; Zhou, X.; Hu, C.; Wang, Y.; Xiao, G.; Zou, B.; Hou, H. Tuning the optical properties of N-aryl benzothiadiazole via Cu(II)-catalyzed intramolecular C-H amination: The impact of the molecular structure on aggregation and solid state luminescence. *Org. Chem. Front.* **2020**, *7*, 3853–3861. [[CrossRef](#)]
44. Wan, L.; Wade, J.; Shi, X.; Xu, S.; Fuchter, M.J.; Campbell, A.J. Highly Efficient Inverted Circularly Polarized Organic Light-Emitting Diodes. *ACS Appl. Mater. Interfaces* **2020**, *12*, 39471–39478. [[CrossRef](#)] [[PubMed](#)]
45. Yan, Z.-P.; Luo, X.-F.; Liu, W.-Q.; Wu, Z.-G.; Liang, X.; Liao, K.; Wang, Y.; Zheng, Y.-X.; Zhou, L.; Zuo, J.-L.; et al. Configurationally Stable Platinahelicene Enantiomers for Efficient Circularly Polarized Phosphorescent Organic Light-Emitting Diodes. *Chem. Eur. J.* **2019**, *25*, 5672–5676. [[CrossRef](#)]
46. Yavari, K.; Delaunay, W.; De Rycke, N.; Reynaldo, T.; Aillard, P.; Srebro-Hooper, M.; Chang, V.Y.; Muller, G.; Tondelier, D.; Geffroy, B.; et al. Phosphahelicenes: From Chiroptical and Photophysical Properties to OLED Applications. *Chem. Eur. J.* **2019**, *25*, 5303–5310. [[CrossRef](#)] [[PubMed](#)]
47. Klimash, A.; Pander, P.; Klooster, W.T.; Coles, S.J.; Data, P.; Dias, F.B.; Skabara, P.J. Intermolecular interactions in molecular crystals and their effect on thermally activated delayed fluorescence of helicene-based emitters. *J. Mater. Chem. C* **2018**, *6*, 10557–10568. [[CrossRef](#)]
48. Jhulki, S.; Mishra, A.K.; Chow, T.J.; Moorthy, J.N. Carbo[5]helicene versus planar phenanthrene as a scaffold for organic materials in OLEDs: The electroluminescence of anthracene-functionalized emissive materials. *New J. Chem.* **2017**, *41*, 14730–14737. [[CrossRef](#)]
49. Chen, T.; Zhang, B.; Liu, Z.; Duan, L.; Dong, G.; Feng, Y.; Luo, X.; Cui, D. Synthesis and properties of thiophene-substituted diaza[7]helicene for application as a blue emitter in organic light-emitting diodes. *Tetrahedron Lett.* **2017**, *58*, 531–535. [[CrossRef](#)]

50. Sahasithiwat, S.; Sooksimuang, T.; Kangkaew, L.; Panchan, W. 3,12-Dimethoxy-5,6,9,10-tetrahydro-7,8-dicyano-[5]helicene as a new emitter for blue and white organic light-emitting diodes. *Dyes Pigm.* **2017**, *136*, 754–760. [[CrossRef](#)]
51. Brandt, J.R.; Wang, X.; Yang, Y.; Campbell, A.J.; Fuchter, M.J. Circularly Polarized Phosphorescent Electroluminescence with a High Dissymmetry Factor from PHOLEDs Based on a Platinahelicene. *J. Am. Chem. Soc.* **2016**, *138*, 9743–9746. [[CrossRef](#)]
52. Hirai, H.; Nakajima, K.; Nakatsuka, S.; Shiren, K.; Ni, J.; Nomura, S.; Ikuta, T.; Hatakeyama, T. One-Step Borylation of 1,3-Diaryloxybenzenes Towards Efficient Materials for Organic Light-Emitting Diodes. *Angew. Chem. Int. Ed.* **2015**, *54*, 13581–13585. [[CrossRef](#)] [[PubMed](#)]
53. Hua, W.; Liu, Z.; Duan, L.; Dong, G.; Qiu, Y.; Zhang, B.; Cui, D.; Tao, X.; Cheng, N.; Liu, Y. Deep-blue electroluminescence from nondoped and doped organic light-emitting diodes (OLEDs) based on a new monoaza[6]helicene. *RSC Adv.* **2015**, *5*, 75–84. [[CrossRef](#)]
54. Shi, L.; Liu, Z.; Dong, G.; Duan, L.; Qiu, Y.; Jia, J.; Guo, W.; Zhao, D.; Cui, D.; Tao, X. Synthesis, Structure, Properties, and Application of a Carbazole-Based Diaza [7] helicene in a Deep-Blue-Emitting OLED. *Chem. Eur. J.* **2012**, *18*, 8092–8099. [[CrossRef](#)]
55. Sahasithiwat, S.; Mophuang, T.; Menbangpung, L.; Kamtonwong, S.; Sooksimuang, T. 3,12-Dimethoxy-7,8-dicyano-[5] helicene as a novel emissive material for organic light-emitting diode. *Synth. Met.* **2010**, *160*, 1148–1152. [[CrossRef](#)]
56. Chen, J.P. [5]-Helicene and dibenzofluorene materials for use in organic light-emitting devices. Patent Application Number PCT/US2002/039350, 10 December 2002.
57. Ma, Z.; Winands, T.; Liang, N.; Meng, D.; Jiang, W.; Doltsinis, N.L.; Wang, Z. A C₂-symmetric triple [5]helicene based on N-annulated triperylene hexaimide for chiroptical electronics. *Sci. China Chem.* **2020**, *63*, 208–214. [[CrossRef](#)]
58. Josse, P.; Favereau, L.; Shen, C.; Dabos-Seignon, S.; Blanchard, P.; Cabanetos, C.; Crassous, J. Enantiopure versus Racemic Naphthalimide End-Capped Helicenic Non-fullerene Electron Acceptors: Impact on Organic Photovoltaics Performance. *Chem. Eur. J.* **2017**, *23*, 6277–6281. [[CrossRef](#)]
59. Lewinska, G.; Danel, K.S.; Sanetra, J. The bulk heterojunction cells based on new helicenes—Preparation, implementation and surface examination. *Sol. Energy* **2016**, *135*, 848–853. [[CrossRef](#)]
60. Dova, D.; Cauteruccio, S.; Manfredi, N.; Prager, S.; Dreuw, A.; Arnaboldi, S.; Mussini, P.R.; Licandro, E.; Abbotto, A. An unconventional helical push-pull system for solar cells. *Dye. Pigm.* **2019**, *161*, 382–388. [[CrossRef](#)]
61. Xu, N.; Zhang, Y.; Fang, L.; Li, T.; Xie, X.; Zhang, J.; Wang, P. A Helical Polycycle Molecular Semiconductor for Durable and Efficient Perovskite Solar Cells. *ACS Mater. Lett.* **2022**, *4*, 11–20. [[CrossRef](#)]
62. Tang, Z.; Li, T.; Cao, Y.; Zhang, Y.; He, L.; Zheng, A.; Lei, M. Chrysene-Based Azahelicene π -Linker of D- π -D-Type Hole-Transporting Materials for Perovskite Solar Cells. *ChemSusChem* **2021**, *14*, 4923–4928. [[CrossRef](#)]
63. Wei, Y.; Zheng, A.; Xie, X.; Zhang, J.; He, L.; Wang, P. A Pyrrole-Bridged Bis(oxa [5] helicene)-Based Molecular Semiconductor for Efficient and Durable Perovskite Solar Cells: Microscopic Insights. *ACS Mater. Lett.* **2021**, *3*, 947–955. [[CrossRef](#)]
64. Lin, Y.-S.; Abate, S.Y.; Wang, C.-I.; Wen, Y.-S.; Chen, C.-I.; Hsu, C.-P.; Chueh, C.-C.; Tao, Y.-T.; Sun, S.-S. Low-Cost Hole-Transporting Materials Based on Carbohelicene for High-Performance Perovskite Solar Cells. *ACS Appl. Mater. Interfaces* **2021**, *13*, 20051–20059. [[CrossRef](#)] [[PubMed](#)]
65. Wang, J.; Wang, Y.; Xie, X.; Ren, Y.; Zhang, B.; He, L.; Zhang, J.; Wang, L.-D.; Wang, P. A Helicene-Based Molecular Semiconductor Enables 85 °C Stable Perovskite Solar Cells. *ACS Energy Lett.* **2021**, *6*, 1764–1772. [[CrossRef](#)]
66. Zheng, A.; Xie, X.; Wang, Y.; Xu, N.; Zhang, J.; Yuan, Y.; Wang, P. A Triple Axial Chirality, Racemic Molecular Semiconductor Based on Thiahelicene and Ethylenedioxythiophene for Perovskite Solar Cells: Microscopic Insights on Performance Enhancement. *Adv. Funct. Mater.* **2021**, *31*, 2009854. [[CrossRef](#)]
67. Wang, J.; Shi, H.; Xu, N.; Zhang, J.; Yuan, Y.; Lei, M.; Wang, L.; Wang, P. Aza [5] helicene Rivals N-Annulated Perylene as π -Linker of D- π -D Typed Hole-Transporters for Perovskite Solar Cells. *Adv. Funct. Mater.* **2020**, *30*, 2002114. [[CrossRef](#)]
68. Xu, N.; Zheng, A.; Wei, Y.; Yuan, Y.; Zhang, J.; Lei, M.; Wang, P. D-p-D molecular semiconductors for perovskite solar cells: The superior role of helical versus planar p-linkers. *Chem. Sci.* **2020**, *11*, 3418–3426. [[CrossRef](#)]
69. Ren, M.; Wang, J.; Xie, X.; Zhang, J.; Wang, P. Double-Helicene-Based Hole-Transporter for Perovskite Solar Cells with 22% Efficiency and Operation Durability. *ACS Energy Lett.* **2019**, *4*, 2683–2688. [[CrossRef](#)]
70. Xu, N.; Li, Y.; Ricciarelli, D.; Wang, J.; Mosconi, E.; Yuan, Y.; De Angelis, F.; Zakeeruddin, S.M.; Gratzel, M.; Wang, P. An Oxa[5]helicene-Based Racemic Semiconducting Glassy Film for Photothermally Stable Perovskite Solar Cells. *iScience* **2019**, *15*, 234–242. [[CrossRef](#)]
71. Lee, C.-C.; Chen, C.-I.; Fang, C.-T.; Huang, P.-Y.; Wu, Y.-T.; Chueh, C.-C. Improving Performance of Perovskite Solar Cells Using [7]Helicenes with Stable Partial Biradical Characters as the Hole-Extraction Layers. *Adv. Funct. Mater.* **2019**, *29*, 1808625. [[CrossRef](#)]
72. Lin, Y.-S.; Abate, S.Y.; Lai, K.-W.; Chu, C.-W.; Lin, Y.-D.; Tao, Y.-T.; Sun, S.-S. New Helicene-Type Hole-Transporting Molecules for High-Performance and Durable Perovskite Solar Cells. *ACS Appl. Mater. Interfaces* **2018**, *10*, 41439–41449. [[CrossRef](#)]
73. Minuti, L.; Taticchi, A.; Marrocchi, A.; Gacs-Baitz, E. Diels-Alder reaction of 3,3',4,4'-tetrahydro-1,1'-binaphthalene. One pot synthesis of a pentahelicenebenzoquinone. *Tetrahedron* **1997**, *53*, 6873–6878. [[CrossRef](#)]
74. Fringuelli, F.; Taticchi, A. Diels Alder reaction. In *Selected Practical Methods*; John Wiley and Sons: New York, NY, USA, 2002.
75. Willmore, N.D.; Liu, L.; Katz, T.J. A Diels–Alder Route to [5]- and [6]-Helicenes. *Angew. Chem. Int. Ed.* **1992**, *31*, 1093–1095. [[CrossRef](#)]

76. Katz, T.J.; Liu, L.; Willmore, N.D.; Fox, J.M.; Rheingold, A.L.; Shi, S.; Nuckolls, C.; Rickman, B.H. An Efficient Synthesis of Functionalized Helicenes. *J. Am. Chem. Soc.* **1997**, *119*, 10054–10063. [[CrossRef](#)]
77. Carreño, M.C.; Hernández-Sánchez, R.; Mahugo, J.; Urbano, A. Enantioselective Approach to Both Enantiomers of Helical Bisquinones. *J. Org. Chem.* **1999**, *64*, 1387–1390. [[CrossRef](#)]
78. Minuti, L.; Taticchi, A.; Marrocchi, A.; Gacs-Baitz, E. A new short route to hexahelicenes. *Synth. Commun.* **1998**, *28*, 2181–2190. [[CrossRef](#)]
79. Minuti, L.; Taticchi, A.; Marrocchi, A.; Gacs-Baitz, E.; Galeazzi, R. An efficient synthetic approach to substituted penta- and hexahelicenes. *Eur. J. Org. Chem.* **1999**, *11*, 3155–3163. [[CrossRef](#)]
80. Marrocchi, A.; Minuti, L.; Taticchi, A.; Dix, I.; Hopf, H.; Jones, P.G.; Gacs-Baitz, E. The preparation of helical cyclophanes containing five-membered rings. *Eur. J. Org. Chem.* **2001**, *22*, 4259–4268. [[CrossRef](#)]
81. Minuti, L.; Taticchi, A.; Lanari, D.; Marrocchi, A.; Gacs-Baitz, E. Synthesis of enantiopure helical cyclophanes containing five-membered heterocyclic rings. *Tetrahedron Asymm.* **2003**, *14*, 2775–2779. [[CrossRef](#)]
82. Minuti, L.; Taticchi, A.; Marrocchi, A.; Lanari, D.; Tesei, I.; Gacs-Baitz, E. Synthesis of helical [2.2]paracyclophanes containing carbocyclic and heterocyclic five-membered rings. *Tetrahedron* **2004**, *60*, 11759–11764.
83. Minuti, L.; Taticchi, A.; Marrocchi, A.; Gacs-Baitz, E. Synthesis of helicenophanes containing two carbocyclic five-membered rings. *Polycycl. Aromat. Compd.* **2005**, *25*, 13–22. [[CrossRef](#)]
84. Minuti, L.; Taticchi, A.; Gacs-Baitz, E.; Marrocchi, A. High pressure Diels-Alder reaction of 2-vinyl-3,4-dihydronaphthalene. Synthesis of cyclopenta[c]- and indeno[c]-phenanthrenones. *Tetrahedron* **1995**, *51*, 8953–8958. [[CrossRef](#)]
85. Yoon, M.-H.; Facchetti, A.; Stern, C.E.; Marks, T.J. Fluorocarbon-Modified Organic Semiconductors: Molecular Architecture, Electronic, and Crystal Structure Tuning of Arene- versus Fluoroarene-Thiophene Oligomer Thin-Film Properties. *J. Am. Chem. Soc.* **2006**, *128*, 5792–5801. [[CrossRef](#)] [[PubMed](#)]
86. Facchetti, A.; Mushrush, M.; Yoon, M.-H.; Hutchison, G.R.; Ratner, M.A.; Marks, T.J. Building Blocks for n-Type Molecular and Polymeric Electronics. Perfluoroalkyl- versus Alkyl-Functionalized Oligothiophenes (nT; n = 2–6). Systematics of Thin Film Microstructure, Semiconductor Performance, and Modeling of Majority Charge Injection in Field-Effect Transistors. *J. Am. Chem. Soc.* **2004**, *126*, 13859–13874. [[PubMed](#)]
87. Chen, L.X.; Shaw, G.B.; Tiede, D.M.; Zuo, X.; Zapol, P.; Redfern, P.C.; Curtiss, L.A.; Sooksimuang, T.; Mandal, B.K. Excited State Dynamics and Structures of Functionalized Phthalocyanines. 1. Self-Regulated Assembly of Zinc Helicenocyanine. *J. Phys. Chem. B* **2005**, *109*, 16598–16609. [[CrossRef](#)]
88. Letizia, J.A.; Cronin, S.; Ponce Ortiz, R.; Facchetti, A.; Ratner, M.A.; Marks, T.J. Phenacyl-Thiophene and Quinone Semiconductors Designed for Solution Processability and Air-Stability in High Mobility n-Channel Field-Effect Transistors. *Chem. Eur. J.* **2010**, *16*, 1911–1928. [[CrossRef](#)]
89. Park, S.H.; Lee, H.S.; Kim, J.-D.; Breiby, D.W.; Kim, E.; Park, Y.D.; Ryu, D.Y.; Lee, D.Y.; Cho, J.H. A polymer brush organic interlayer improves the overlying pentacene nanostructure and organic field-effect transistor performance. *J. Mater. Chem.* **2011**, *21*, 15580–15586. [[CrossRef](#)]
90. Dolomanov, O.V.; Bourhis, L.J.; Gildea, R.J.; Howard, J.A.K.; Puschmann, H. OLEX2: A complete structure solution, refinement and analysis program. *J. Appl. Cryst.* **2009**, *42*, 339–341. [[CrossRef](#)]
91. Sheldrick, G.M. A short history of SHELX. *Acta Crystallogr. A* **2008**, *A64*, 112–122. [[CrossRef](#)]
92. Skaisgiris, R.; Serevičius, T.; Dodonova, J.; Banevičius, D.; Kazlauskas, K.; Tumkevičius, S.; Juršėnas, S. Tuning of HOMO-LUMO localization for achieving thermally activated delayed fluorescence. *J. Lumin.* **2022**, *241*, 118473. [[CrossRef](#)]